2020 IEEE/RSJ International Conference on Intelligent Robots and Systems (IROS)
October 25-29, 2020, Las Vegas, NV, USA (Virtual)

A novel and controllable cell-based microrobot in real vascular network for target tumor therapy

Yanmin Feng, Lin Feng*, Yuguo Dai, Xue Bai, Chaonan Zhang, Yuanyuan Chen and Fumihito Arai

Abstract— **Magnetic microrobots can be propelled precisely and wirelessly *in vivo* using magnetic field for targeted drug delivery and early detection. They are promising for clinical trials since magnetic fields are capable of penetrating most materials with minimal interaction, and are nearly harmless to human beings. However, challenges like the biocompatibility, biodegradation and therapeutic effects of these robots must be resolved before this technique is allowed for preclinical development. In this study, we proposed a cell-robot based on macrophages for carrying drugs to kill tumors propelled by magnetic gradient-based pulling. A custom-designed system with strong gradient magnetic field system in three-dimensional (3D) space using the minimum number of coils is used for precise control of the cell-based microrobot. The cell-based microrobots were fabricated by assembling magnetic nanoparticles (Fe3O4), anti-cancer drugs (DOX) into macrophages for magnetic actuation and therapeutic effects. Vitro experiments show that cell-based microrobots can be accurately transported to the destination or approaching a targeted cancer cell. The magnetic nanoparticles have negligible effects on the cell-based microrobot and the organism, which makes the cell-based microrobot safe for *in vivo* experiments. The carried drugs in the cell-based microrobot can be released by the irradiation of the near-field infrared and kill the cancer cells. Further *in vivo* experiments prove that the cell-based microrobot can be transported to tumor area and release drugs to kill cancer effectively. The research provides biocompatible and biodegradable cell-based microrobots for early tumor prevention and targeted precision therapy.**

I. INTRODUCTION

Cancer is the leading cause of death worldwide and is still an unsolved mystery in the medical field. Although immunotherapy has made a remarkable progress especially for cancer treatment, it is still very far from being a powerful therapeutic tool. Therefore, current clinical cancer therapies primarily rely on traditional approaches such as surgical resection, radiotherapy, and chemotherapy. It is well known that these approaches bear the risks of destruction of normal cells and healthy tissues, disturbance of the immune system, and an enhanced recurrence incidence. Consequently, precise therapeutic delivery to the target sites without damaging normal cells is a goal of modern medicine.

With the tremendous advancement of micro/nano manufacturing technology, it has reached nano-level accuracy, which has promoted the development of microrobot technology. Several researchers have developed a variety of micro/nanorobots [1-6]. However, most of these studies focused on the controllable operation of microrobot for *in vitro* applications [7, 8], and very few *in vivo* studies such as in the eyeballs or stomach [9, 10] have been reported. Further, the curative effect is extremely limited. In addition, these microrobots are depend on the characteristics of biomaterials and accuracy of three-dimensional (3D) printers, which makes them highly expensive. Modified magnetic nanoparticles (MNPs) containing therapeutic agents have been used and proved to be effective for cancer treatment with limited side effects [11, 12]. However, this method has some limitations in tumor therapy primarily because it depends on the leakage property of tumor vessels, which restricts the penetration of nanoparticles into the avascular central region of a tumor. Therefore, *in vitro* and *in vivo* control of these robots requires further refinement and optimization [13].

Magnetic field can propel the microrobots precisely and wirelessly *in vivo* for targeted drug delivery and early detection [14, 15].Although drug-based chemotherapy is

* This work was supported by the Natural Science Foundation of Beijing (Grant No.17L20128), and the National Key R&D Program of China (Grant No.2019YFB1309702).

Lin Feng, Deyuan Zhang, Yanmin Feng and Yuanyuan Chen are with School of Mechanical Engineering & Automation, Beihang University, Beijing 100191, China and also with Beijing Advanced Innovation Center for Biomedical Engineering, Bei hang University, Beijing 100083, China. (e-mail: linfeng@buaa.edu.cn; zhangdy@buaa.edu.cn; fengyanmin@buaa.edu.cn; chenyuanyuan0526@sina.com;).

Xue Bai, Yuguo Dai and Chaonan Zhang are with School of Mechanical Engineering & Automation, Beihang University, Beijing 100191, China. (e-mail: baixue041104@163.com; daiyuguo5612@163.com; zhangchaonan_bit@163.com).

Fumihito Arai is with Department of Micro-Nano System Engineering, Nagoya University, Furo-cho, Chikusa-ku, Nagoya, 464-8603, Japan. (e-mail: arai@mech.nagoya-u.ac.jp).

restricted by several undesirable effects such as its safe dosage and drug resistance of some cancer cells, which influence its therapeutic efficacy, it is still considered as the main route for cancer treatment [16]. In contrast, microrobot propelled by a magnetic field can deliver the drugs directly to the tumor site with minimal effect on the other tissues, which effectively increases the local drug concentration. Furthermore, magnetic-field controlled drug delivery can be used to enhance the drug targets through the penetration into cellular blockages such as brain blood barriers to effectively reach the nearly inaccessible tumorous zone with less side effects [17]. Preclinical studies have demonstrated that magnetic cell therapy can lead to 1.5-3.0 fold greater cell delivery to a target region and a sustained cell population as compared to non-magnetic cell therapy [18]. However, these robots may be treated as foreign body and can induce an immune rejection. Modification of these robots using various cell membranes is an effective approach to overcome this problem.

Here, we have introduced a cell-based microrobot based on macrophages for carrying drugs to kill the tumors *in vivo* using magnetic-gradient based pulling. These cell-based microrobots were fabricated by assembling MNPs and anti-cancer drugs into macrophages for magnetic actuation and therapeutic effects. Accordingly, the biocompatibility and biodegradation issues with respect to other microrobots were observed to be minimal. Our findings suggested that the cell-based microrobots can be accurately transported to the destination, i.e., the target cancer cell. The MNPs have a negligible effect on the cell-based microrobot and the organism, which makes the cell-based microrobot safe for *in vivo* experiments as well. The drugs carried by the cell-based microrobot was released by irradiation with a the near-infrared (NIR) light to destroy the cancer cells. Further, *in vivo* experiments suggested that the cell-based microrobot can be transported to tumor area to effectively release the drugs and destroy the cancer cells. Overall, our study provides a novel route toward the development of biocompatible and biodegradable cell-based microrobots for early tumor prevention and targeted cancer therapy.

II. Methods and Materials

A. *Fabrication of cell-based microrobot*

MNPs containing Fe3O4 and DOX were prepared for cellular internalization. The biocompatible drug-loaded MNPs were synthesized using rotating evaporation method.

The dosage of DOX drug was confirmed by evaluating the ultraviolet absorption of DOX at different concentration using 480-nm absorption wavelength. The relationship between concentration and absorbance was as follows: Concentration = 0.8226 × Absorbance + 0.0037 The concentration of DOX in the sample was 0.119 mg/mL according to the above equation. All these results suggest that the drug-loaded MNPs containing 0.119 mg/ml DOX and 1 mg/ml Fe3O4 were successfully fabricated.

B. Cell culture

Mouse macrophage cell line, RAW264.7, was purchased from National Infrastructure of Cell Line Resource and maintained in high glucose DMEM supplemented with 10% FBS (GIBCO). Cancer cells and human breast adenocarcinoma cell line (MCF-7) were also cultured in high glucose DMEM medium containing 10% FBS, 1% penicillin and streptomycin, and 1% non-essential amino acids. These cell lines were incubated at 37°C under 5% CO2 in a humid chamber. The cells were dissociated using 0.05 % trypsin-EDTA (GIBCO). All cells were centrifuged at 600 g for 6 min and the pellets were suspended in the growth medium.

C. Evaluation of the New Driven Method

An electromagnetic actuation (EMA) system was adopted for the external active actuation of the macrophage-based microrobot. As shown in Fig. 5, the magnetic system was driven by a computer, an AD/DA module (using USB-6211 data acquisition system: National Instruments Inc., USA), four digital drivers (DZRALTE-040L080 motor driver: AMD, USA), four DC power supplies, and magnetic field generator. The computer control was based on Visual Studio 2010 (C# language) to generate digital signals, which were then converted into analog signals by the AD/DA conversion modules. The drivers sent the desired current to the electromagnets and generated the required magnetic field in the working area.

D. In vitro force analysis of cell-based microrobot in the system

As the cell-based microrobots were manufactured on a mouse macrophage template, its density was close to that of the culture medium, enabling the gravitational and buoyant forces to be offset. Under a magnetic field, the cell-based microrobot is primarily affected by the magnetic force and the resistance of the culture solution. The magnetic force applied to the cellular robot can be calculated as follows:

$$F_{drag} = (m_{cell} \cdot \nabla)B = m_{cell} * \nabla B \quad (1)$$

where m_{cell} is the magnetization vector of the cell-based microrobot. As the gradient field in the working area is nearly uniform, ∇B can be treated as a constant. The resistance of the cell-based microrobot in the medium can be calculated by approximating the robot as a sphere [19], i.e.,

$$F_{resistance} = C_D A \frac{\rho u^2}{2} \quad (2)$$

where $A = \pi R^2$ represents the cross-sectional area of the cell-based microrobot, R is its diameter, u is the speed, ρ is the density of the solution, $C_D = \frac{12\mu}{\rho R u}$ is the drag coefficient, and μ is the kinematic viscosity of the liquid. Thus, the viscous resistance can be rewritten as

$$F_{resistance} = 6\pi\mu R u \quad (3)$$

When the cell-based microrobot moves steadily, the magnetic force acting on the robot is equal to the liquid resistance, i.e., $F_{drag} + F_{resistance} = 0$.

E. In vivo tumor destruction

All the animal protocols were approved by the Biological and Medical Ethics Committee of Beijing University of Aeronautics and Astronautics. Mice were housed in stainless steel cages containing sterile paddy husk as bedding in ventilated rooms with free access to water and commercial food.

Eight-week-old female Bal b/c nude mice with a weight of about 16-18 g was injected by MCF-7 tumor cells into the dorsum adjacent to the tail at a concentration of 1×107 (200 mL). At the tumor volume of ~100 mm3, the magnetized cell-based microrobot were intravenously injected and randomly divided into two groups (three mice per group), which were called target group and non-target group. The magnetic field was applied in the position of tumor for 2 h. A small animal fluorescence imaging system with 705-nm excitation wavelength and a 735-nm filter was used to record the images at different time points. Then, the magnetized cell-based robot were intravenously administrated 3 times every 5 day. The tumors sites of mice were exposed to a NIR laser (808 nm, 2.5 W/cm^2) for 8 min after 2 h exposure to the magnetized field at a laser intensity, which was least harmful to the skin. Tumor weight was then measured. In addition, the toxicity was determined by monitoring animal behavior and the weight loss. Morphological changes were observed using a microscope (Leica, Germany).

III. Results

A. Control strategy and design of cell-based microrobots

Figure 1 shows a schematic for the design of magnetized cell-based macrophage for active and targeted delivery of anticancer drugs to a solid tumor. Magnetized cell-based microrobots were fabricated using the internalization properties of the immune cells by co-incubating macrophages and MNPs [20, 21]. The macrophage-based microrobots were designed to facilitate hybrid actuation through active tumor targeting by a magnetic control system and infiltration into the tumor tissue by macrophage recruitment. Using the self-actuating abilities of the macrophages, these microrobots were able to infiltrate into the tumor tissue and release the loaded therapeutic agents.

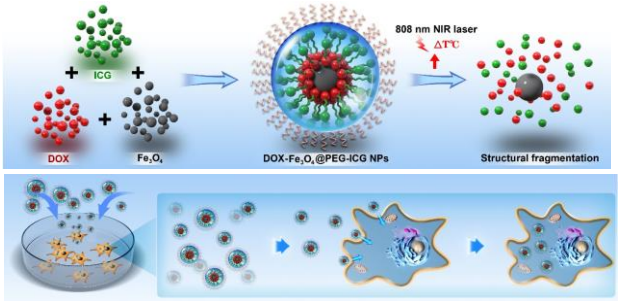

Figure 1. Schematic of macrophage-based microrobot with MNPs.

B. Evaluation of magnetized cell-based microrobots

The internalization of drug-loaded MNPs into the macrophages was accomplished through phagocytosis of the macrophages, which was induced by co-culturing them. As macrophages exhibit an intrinsic phagocytosis capacity, drug-loaded MNPs can be easily embedded into them. Figure 2 shows that drug-loaded MNPs are internalized into the cytoplasm of magnetized cell-based microrobots through the indocyanine green (ICG) signals. Further, the accumulative drug release of doxorubicin (DOX) from the magnetized cell-based microrobots after NIR irradiation is shown in Fig. 3. These results confirm the successful fabrication of NIR sensitive magnetized cell-based microrobots for chemotherapeutic functions.

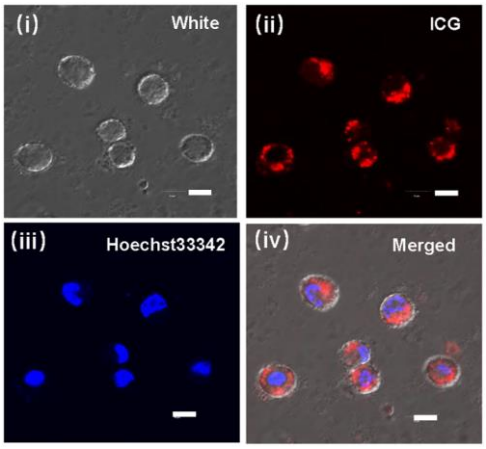

Figure 2. Identification of intracellular fluorescence from drug-loaded nanoparticles by confocal microscopy. The horizontal bar indicates 10 μm.

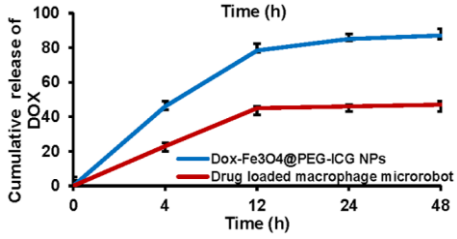

Figure 3. Cumulative release rate of DOX from macrophage-based microrobot with DOX-PEG-ICG-Fe3O4 nanoparticles.

To evaluate the photothermal performance of the MNPs, NIR laser was chosen as the light source. NIR is often used in photothermal therapy (PTT) because the light absorption of tissue chromophores is minimum in the NIR region. Different concentrations (0 ng/ml, 5 ng/ml, 10 ng/ml, 20 ng/ml, and 40 ng/ml) of the drug-loaded MNPs were irradiated with 808-nm NIR laser (2.5 W/cm2) for 10 min, and the temperature variation was determined as a function of the irradiation time (Fig. 4A). The results suggest that the temperature variation in pure water is almost negligible. However, the temperature rapidly increases with increasing concentration of NPs as well as with increasing irradiation time. This effect is more prominent in first 6 min and becomes inconspicuous with further increase up to 10 min (Fig. 4B). For the MNPs with a concentration of 20 ng/ml, the temperature increased from 25 to 56.2 ℃ in 6 min, indicating a rapid and efficient conversion of NIR energy into thermal energy. As the concentration is further increased, no distinct improvement in the photothermal performance was observed. Based on these observations, 20 ng/ml was chosen as a proper concentration for further evaluation. To investigate the effect of laser intensity on the temperature variation, 20 ng/ml of MNPs dispersed in water were exposed to the laser at laser intensity of 1 W/cm2, 2 W/cm2, 2.5 W/cm2, 3 W/cm2, and 3.5 W/cm2 for 10 min. The photothermal heating curve indicates a distinct laser-power-dependent photothermal effect for MNPs (Fig. 4B). Specifically, temperatures at 2.5 W/cm2 and 3 W/cm2 were around 56.2 ℃ and 58.5 ℃, respectively. As the temperature at the laser intensity of 2.5 W/cm2 was found to be enough for PTT, it was chosen as the laser intensity for further experiments. Generally, 42℃ is sufficient to induce target cell death.

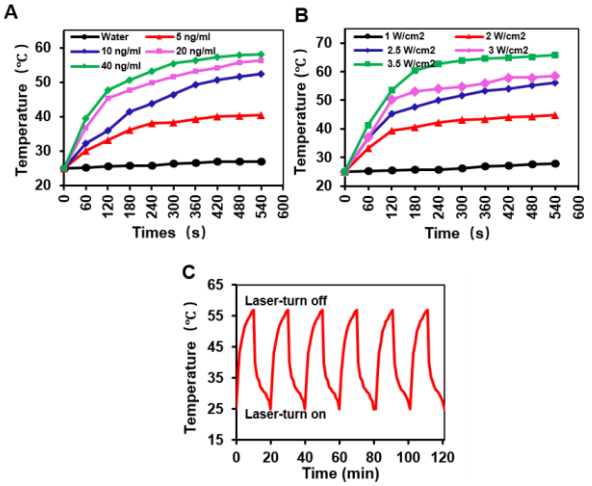

Figure 4. (A) Variation in the temperature as a function of the concentration of nanoparticles. (B) Effect of different power densities of 1, 2, 2.5, 3, 3.5 W/cm^2 for 10 mins on temperature. (C) Stability test of nanoparticles. Temperature changes of the drug loaded nanoparticles over 6 cycles of irradiation/cooling.

In addition to the photothermal conversion capability, photothermal stability is a significant factor during PTT. The temperature profiles were evaluated for six successive cycles of heating/cooling processes (Fig. 4C). The results suggest that the temperature elevation was perfectly maintained during the six cycles of testing. This confirms the highly stable photothermal conversion ability of drug-loaded MNPs. Consequently, the remarkable photothermal conversion efficiency as well as stability further support the utilization of MNPs as an excellent candidate for PTT applications.

C. Magnetic control of the cell-based microrobot in vitro

It was expected that the magnetized cell-based microrobots exhibit tumor-targeting properties because the macrophages possess innate tumor-infiltration characteristics and macrophage-based microrobots with internalized MNPs can be manipulated using an electromagnetic control system. To guide the macrophage-based microrobots to the sites of interest, *in vitro* experiments were performed using a self-constructed electromagnetic control system, as shown in Fig. 5A. The control system consists of four electromagnets. The angle between any two magnets is same: $arc\cos(-1/3)$, indicating a high symmetry of the system. The system can generate a strong gradient field in the central working area, which can propel the cell-based microrobot by the magnetic-gradient based pulling forces. Fig. 5B shows the distribution of the field, where only the coil G is energized. It is evident that the magnitude of ∇B is nearly constant in the central area. This explains why the magnetic agents are ideally manipulated in the central region with a nearly uniform gradient.

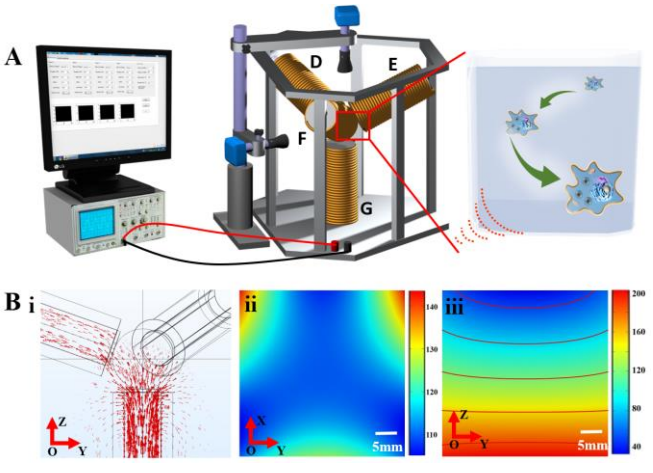

Figure 5. Designed electromagnetic system. (A)Schematic of the system. (B) Distribution of magnetic field, where only electromagnet G is energized at IG = 15 A. (i) Distribution of magnetic induction lines. (ii) Top view and (iii) side view of the distribution of the magnetic field in the central area. Red lines represent the field contours (uniform gradient field).

As shown in Fig. 6, the fabricated magnetized cell-based microrobots were propelled by the magnetic system moving along a triangular path toward the three positions marked as a, b, and c. The actual position perfectly matches with the planned pathway. The distance between the cell-based microrobot and the desired position converges to zero as it moves along the planned path.

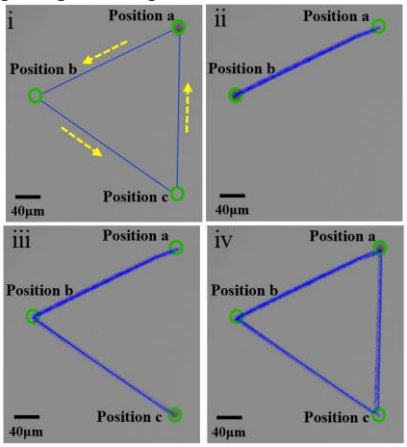

Figure 6. *In vitro* control of cell-based microrobot. (i) Planned path of the cell-based microrobot. (ii)-(iv) Real path of the cell-based microrobot in the cell culture medium.

D. Confirmation of tumor-killing effect of the cell-based microrobot in vitro

To assess the therapeutic capacity of the magnetized cell based microrobot towards MCF-7 cells by carried drugs *in vitro*, MTT assay and live/dead cell staining were further carried out (Fig. 7). When it was employed in the PTT, the cancer cells were killed completely, which can be verified by Calcein-AM/PI staining, showing a red fluorescence of dead cells.

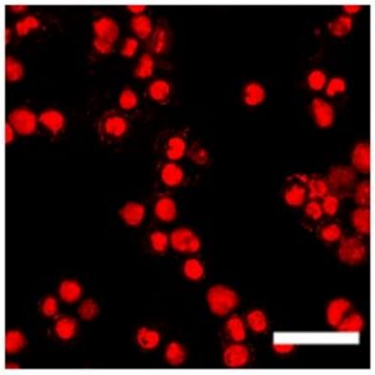

Figure 7. Cancer cells killing efficiency by cell-based microrobot. The horizontal bar indicates 50 μm. Green and red colors represent live and dead cells.

E. Precise in vivo destruction of tumor under magnetic field

To assess the effect of magnetized cell-based microrobots on MCF-7 tumor-bearing mice *in vivo*, the mice were classified into magnet targeted and non-targeted groups. The tail vein of the mice was injected with magnetized cell-based microrobots and the tumor site was placed on the magnet for 2 h for exposure to the magnetic field. The distribution of magnetized cell-based microrobots after magnetic interaction was evaluated *in vivo* by monitoring the accumulation of circulating ICG using a small animal imaging system. In addition, to confirm the effect of cell-based microrobots subjected to the magnetic field in *vivo*, the tail was placed on the magnet for 2 h after tail vein injection of cell microrobots. The accumulation of ICG signals at the position of magnet was observed. Overall, these results demonstrate that an external magnetic field can induce local accumulation of magnetized cell-based microrobots in the target tissue.

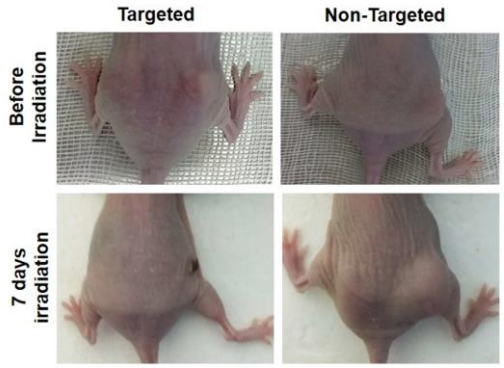

Figure 8. *In vivo* suppression of tumors under magnet target or non-magnet target after NIR irradiation. Representative images of mice bearing MCF-7 tumors magnet target and non-magnet target (after 7 days).

As shown in Fig. 8, after NIR laser irradiation for 8 mins (808 nm, 2.5 W/cm2), tumors in the non-target group grew rapidly, indicating that the irradiation did not affect MCF-7 tumor growth. However, the tumors in the target group were significantly inhibited after irradiation. The obvious difference between both groups was observed after and 7 days of irradiation, where almost complete tumor regression with a tumor weight of 0.053 g (Fig. 9) was observed. This indicate that magnetized cell-based microrobots can suppress MCF-7 tumor growth after irradiation for drug release. There were almost no intact tumor cells, indicating an inspiring therapeutic effect. However, the long-term toxicity of magnetized cell-based microrobots still needs to be evaluated for clinical application.

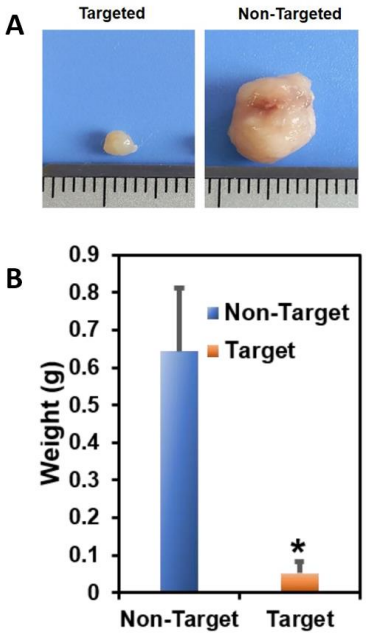

Figure 9. (A) Digital images of excised tumors from the mouse after seven days of NIR irradiation. (B) Weight of tumor tissue after seven days of irradiation. Here, n = 5 and $p < 0.05$ (*).

IV. Conclusion

In this paper, we successfully proposed an innovative cell-based microrobot for targeted cancer therapy. This cell-based microrobot can be precisely controlled by magnetic system *in vitro* and *in vivo*. Furthermore, the drug loaded cell-based microrobot can destruct tumor *in vivo* under magnetic field. This has promising prospect for clinical surgery in the future.

References

[1] H. Xie *et al.*, "Reconfigurable magnetic microrobot swarm: Multimode transformation, locomotion, and manipulation," *Science Robotics,* vol. 4, no. 28, p. eaav8006, 2019.

[2] S. Jeon *et al.*, "Magnetically actuated microrobots as a platform for stem cell transplantation," *Science Robotics,* vol. 4, no. 30, p. eaav4317, 2019.

[3] J. Li *et al.*, "Development of a magnetic microrobot for carrying and delivering targeted cells," *Science Robotics,* vol. 3, no. 19, p. eaat8829, 2018.

[4] L. Feng *et al.*, "On-chip microfluid induced by oscillation of microrobot for noncontact cell transportation," (in English), *Applied Physics Letters,* vol. 111, no. 20, Nov 13 2017.

[5] S. Tasoglu, E. Diller, S. Guven, M. Sitti, and U. Demirci, "Untethered micro-robotic coding of three-dimensional material composition," (in English), *Nature Communications,* vol. 5, Jan 2014.

[6] A. Snezhko and I. S. Aranson, "Magnetic manipulation of self-assembled colloidal asters," (in English), *Nature Materials,* vol. 10, no. 9, pp. 698-703, Sep 2011.

[7] F. Guzman-Lastra, A. Kaiser, and H. Lowen, "Fission and fusion scenarios for magnetic microswimmer clusters," (in English), *Nature Communications,* vol. 7, Nov 22 2016.

[8] D. Kokkinis, M. Schaffner, and A. R. Studart, "Multimaterial magnetically assisted 3D printing of composite materials," (in English), *Nature Communications,* vol. 6, Oct 2015.

[9] G. Chatzipirpiridis *et al.*, "Electroforming of implantable tubular magnetic microrobots for wireless ophthalmologic applications," *Adv Healthc Mater,* vol. 4, no. 2, pp. 209-14, Jan 28 2015.

[10] X. Yan *et al.*, "Multifunctional biohybrid magnetite microrobots for imaging-guided therapy," *Science Robotics,* vol. 2, no. 12, p. eaaq1155, 2017.

[11] H. Y. Kim *et al.*, "Therapeutic Efficacy-Potentiated and Diseased Organ-Targeting Nanovesicles Derived from Mesenchymal Stem Cells for Spinal Cord Injury Treatment," (in English), *Nano Letters,* vol. 18, no. 8, pp. 4965-4975, Aug 2018.

[12] S. Zanganeh *et al.*, "Iron oxide nanoparticles inhibit tumour growth by inducing pro-inflammatory macrophage polarization in tumour tissues," (in English), *Nature Nanotechnology,* vol. 11, no. 11, pp. 986-994, Nov 2016.

[13] S. E. Chung, X. G. Dong, and M. Sitti, "Three-dimensional heterogeneous assembly of coded microgels using an untethered mobile microgripper," (in English), *Lab on a Chip,* vol. 15, no. 7, pp. 1667-1676, 2015.

[14] W. Q. Hu, G. Z. Lum, M. Mastrangeli, and M. Sitti, "Small-scale soft-bodied robot with multimodal locomotion," (in English), *Nature,* vol. 554, no. 7690, pp. 81-85, Feb 1 2018.

[15] W. Gao *et al.*, "Cargo-Towing Fuel-Free Magnetic Nanoswimmers for Targeted Drug Delivery," (in English), *Small,* vol. 8, no. 3, pp. 460-467, Feb 6 2012.

[16] X. Wang *et al.*, "Facile Fabrication of Magnetic Microrobots Based on Spirulina Templates for Targeted Delivery and Synergistic Chemo-Photothermal Therapy," (in English), *Acs Applied Materials & Interfaces,* vol. 11, no. 5, pp. 4745-4756, Feb 6 2019.

[17] B. Chertok *et al.*, "Iron oxide nanoparticles as a drug delivery vehicle for MRI monitored magnetic targeting of brain tumors," *Biomaterials,* vol. 29, no. 4, pp. 487-96, Feb 2008.

[18] S. T. Grivna, E. Beyret, Z. Wang, and H. Lin, "A novel class of small RNAs in mouse spermatogenic cells," (in eng), *Genes Dev,* Research Support, N.I.H., Extramural vol. 20, no. 13, pp. 1709-14, Jul 1 2006.

[19] G. K Batchelor, *An Introduction to Fluid Dynamic*. Cambridge University Press, 1967.

[20] J. Han *et al.*, "Hybrid-Actuating Macrophage-Based Microrobots for Active Cancer Therapy," *Sci Rep,* vol. 6, p. 28717, Jun 27 2016.

[21] D. L. J. Thorek and A. Tsourkas, "Size, charge and concentration dependent uptake of iron oxide particles by non-phagocytic cells," *Biomaterials,* vol. 29, no. 26, pp. 3583-3590, 2008.